Terrestrial Magma Ocean Solidification and Formation of a Candidate D″ Layer

by

Alessondra Springmann

B.A., Wellesley College (2007)

Submitted to the
Department of Earth, Atmospheric, and Planetary Sciences
in partial fulfillment of the requirements for the degree of

Master of Science in Earth and Planetary Sciences

at the

MASSACHUSETTS INSTITUTE OF TECHNOLOGY

June 2011

Author .....

Department of Earth, Atmospheric, and Planetary Sciences
May 18, 2011

Certified by .....
Linda T. Elkins-Tanton
Assistant Professor
Thesis Supervisor

Accepted by .....
Maria T. Zuber
E. A. Griswold Professor of Geophysics
Head of the Department

Terrestrial Magma Ocean Solidification and Formation of a Candidate D″ Layer

by

Alessondra Springmann

Submitted to the
Department of Earth, Atmospheric, and Planetary Sciences
on May 18, 2011, in partial fulfillment of the
requirements for the degree of
Master of Science in Earth and Planetary Sciences

Abstract

In this thesis we investigate the solidification of early magma oceans on the Earth and the formation of a deep dense layer at the core-mantle boundary. We also study the concentrations and densities of the last layers of the solidified magma ocean and how they create a deep dense layer after solid-state overturn. The deep dense layer that forms in our model matches the bulk physical properties of the D″ layer observed by other workers. This layer is also sufficiently dense that the bulk of its material is not reentrained by the mantle after the onset of convection, and that this layer is enriched in incompatible elements such as samarium and neodymium regardless of distribution coefficients used for incompatible elements in mantle minerals such as perovskite. However, we found that this probable D″ layer is more enriched in samarium than is to be expected for a planet's mantle which evolves from an initially chondritic composition.

Thesis Supervisor: Linda T. Elkins-Tanton
Title: Assistant Professor

Acknowledgments

Foremost, I am grateful for my research and academic advisors, Linda T. Elkins-Tanton and Richard Binzel. Their patience and willingness to explain concepts to me has been invaluable. Richard W. Carlson's guidance and time regarding incompatible element behaviors were incredibly helpful and generous. James L. Elliot, Miri E. Skolnik, Richard G. French, Paul R. Weissman, Blanche E. Staton, Jane A. Connor, and Judith Tripp deserve acknowledgment for their support as well.

Regarding content and structure, Susan D. Benecchi's detailed comments went above and beyond the call of duty; I am grateful for her continued guidance and mentoring. Andrew D. Wickert, Mariela C. Perignon, and Francesca E. DeMeo provided edits and useful conversations. Matthew F. Lockhart has been the best officemate I could ask for; this paper owes a good deal to his presence. Emily C. Davidson provided insight into mass balance, isotopes of rare-Earth elements, and the motivation necessary to continue working on this project. Zachary J. Bailey has listened consistently and compassionately when he was not providing more Wagner and puns than should be allowed by law—thank you for the gneiss hikes.

On the technical side, Karl C. Ramm introduced me to Ubuntu; David S. Glasser provided useful conversations about `git` and version control; and Kevin A. Riggle enabled more consistent server uptime. Tim D. Smith and Benjamin J. Kaduk provided conversations about isotopes and moles.

While I learned about the differences between barium sulfate and barite, Jan Hanson, Uma Mahadevan, Douglas A. Corley, and William Prange helped me to better appreciate Group II minerals. Robin Winn also deserves thanks for teaching relaxation techniques.

The Inverness Yacht Club remains a second home, and I am especially grateful for the generosity and care of the Darley and Biller families. The support of my parents, Toni Littlejohn and Christopher Springmann, has been unwavering. Eric B. Holmes brought three important things to this thesis: trips to the UC Davis geology library, a relentlessly positive big-picture outlook, and focused encouragement. He was instrumental in providing specific feedback, clarifying my thought and writing processes, and ultimately seeing this project worked on and completed.

This research was partially supported by an NSF Astronomy grant to L. T. Elkins-Tanton.

With apologies to Hunter S. Thompson:

"We can't stop here. This is adiabat country!"

In Memory of James Elliot

1943–2011

Teacher, mentor, and friend

1 Introduction

Terrestrial planets likely formed by accretion of differentiated planetary embryos and by sweeping up planetesimals that remain after planetary embryo formation (Chambers, 2004; Canup, 2008; Raymond *et al.*, 2009, and references therein). The heat of accretion caused material in the upper portions of early terrestrial planets' mantles to melt (Safronov, 1978; Weidenschilling *et al.*, 1997). With each planetary embryo collision, the proto-Earth's mantle likely melted and differentiated, resulting in the mantle having gone through the differentiation and melting process numerous times.

Little evidence remains from Earth's early history, as it has been erased by billions of years of mantle convection and plate tectonics. Among many others, there are two specific measurements made on the modern Earth that may be explained by magma ocean processes: the existence of a dense layer at Earth's core-mantle boundary, as well as the concentrations of rare-Earth elements in rocks extracted from the mantle.

At present, Earth has a structure characterized by layers: crust, mantle, and a dense region at the core-mantle boundary (CMB), and likely "acquired its primary layered structure... very early in its history," (Lay *et al.*, 1998) including the stratification present at the CMB. The lowermost layer in the mantle above the core is known as the D″ layer (Figure 1), and has a host of physical characteristics (density, thickness) that distinguish it from the surrounding layers inside the Earth, detectable through seismic studies (Garnero, 2000).

There is evidence that a mineralogical phase change occurs in the D″ layer, making it physically distinct from the mantle above it (Oganov and Ono, 2004). It has been suggested that the D″ layer could be a graveyard for slab "dregs" (Garnero, 2000). Regardless of what explains the seismic discontinuities in this region of the Earth, it is likely this layer has a very high density, in contrast with the mantle (Lay *et al.*, 1998). Various models predict the D″ layer to be from 150 km to 300 km in thickness (Kendall and Shearer, 1994; Garnero, 2000; Oganov and Ono, 2004; Wentzcovitch *et al.*, 2006), while tomographic inversion studies show the heterogeneity of this layer (Garnero, 2000).

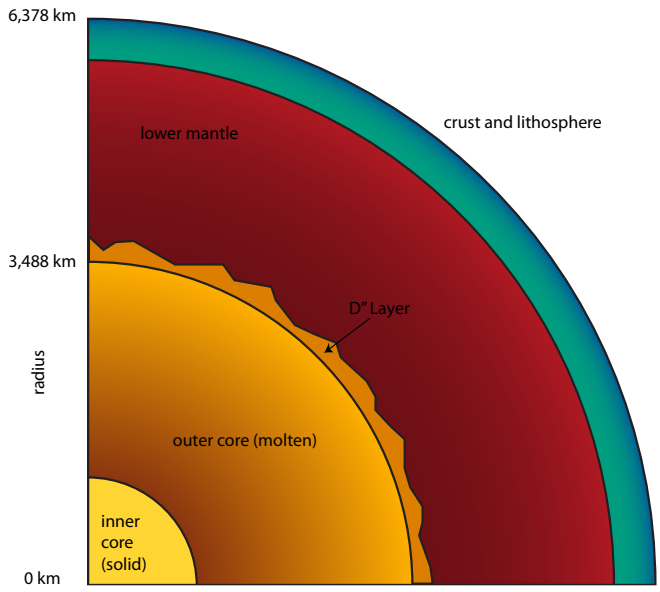

Figure 1: A cartoon of the interior of the Earth, showing the core, mantle, and crust, with the D″ layer at the core-mantle boundary. Adapted from Beatty *et al.* (1999).

The decay of 146-samarium to 142-neodymium can provide insights into early events in Earth's history. This decay chain is used because 146-samarium was produced in significant amounts during the supernova event that created our solar system (Maji *et al.*, 2006), and has a half-life of 1.03×10^8 years (Lugmair *et al.*, 1983). Due to the length of its half-life, all 146-samarium present at the beginning of the solar system decayed to 142-neodymium during the first 400-500 Ma of Earth's history and thus these isotopes are useful for investigating early mantle events (Rollinson, 2007).

The relative abundances of samarium and neodymium in Earth's mantle should not be affected by the formation of Earth's core or volatile loss during terrestrial accretion (Boyet and Carlson, 2005). Not only extremely similar in terms of compatibility because of their similar radius and valence states, samarium and neodymium are both lithophile elements (Amelin and Rotenberg, 2004)–that is, they are elements concentrated in Earths crust and mantle (as opposed to the terrestrial core). Sm and Nd are also refractory, having high condensation temperatures of approximately 1400°C (Carlson and Boyet, 2008). As both are lithophile and refractory elements,

their relative abundances in terrestrial rocks should remain unchanged despite events such as core formation or weathering; thus we assume that their abundance ratios are similar to both solar system and bulk planetary values (Amelin and Rotenberg, 2004).

DePaolo and Wasserburg (1976) measured the neodymium isotope abundances in terrestrial rocks and found that they followed the average abundances of neodymium isotopes in chondrite meteorites, which are believed to be the building blocks of Earth (Ringwood, 1966). As terrestrial neodymium departures from chondritic values are small, DePaolo and Wasserburg (1976) use epsilon notation (Equation 1) to measure neodymium concentration deviations in samples from terrestrial standards (Boyet and Carlson, 2005). Crustal rocks, which have been extracted from the mantle, have a ϵ^{142}Nd value of 0 compared to the terrestrial La Jolla standard, while chondrites have a negative ϵ^{142}Nd value (DePaolo and Wasserburg, 1976; Boyet and Carlson, 2005; Carlson and Boyet, 2008). Figure 2 shows deviations in ^{142}Nd/^{144}Nd for a variety of meteorites, compared to a terrestrial standard for neodymium in units of μ^{142}Nd (Equation 2), which has a multiplier of 1,000,000 instead of 10,000 as for ϵ^{142}Nd.

$$\epsilon^{142}\mathrm{Nd} = \left[\frac{\left(\frac{^{142}\mathrm{Nd}}{^{144}\mathrm{Nd}}\right)_{sample}}{\left(\frac{^{142}\mathrm{Nd}}{^{144}\mathrm{Nd}}\right)_{standard}} - 1 \right] \times 10,000 \tag{1}$$

$$\mu^{142}\mathrm{Nd} = \left[\frac{\left(\frac{^{142}\mathrm{Nd}}{^{144}\mathrm{Nd}}\right)_{sample}}{\left(\frac{^{142}\mathrm{Nd}}{^{144}\mathrm{Nd}}\right)_{standard}} - 1 \right] \times 1,000,000 \tag{2}$$

If the Earth formed primarily from chondrite meteorites, and the relative abundances of the lithophiles samarium and neodymium were not affected by core formation, then there should be no appreciable difference between ϵ^{142}Nd values of terrestrial samples and chondrites.

However, there is a difference between the ϵ^{142}Nd values of terrestrial rocks and chondrite meteorites that cannot be resolved. There are two possible explanations: one, that Earth formed out of a different class of meteorites with an ϵ^{142}Nd value

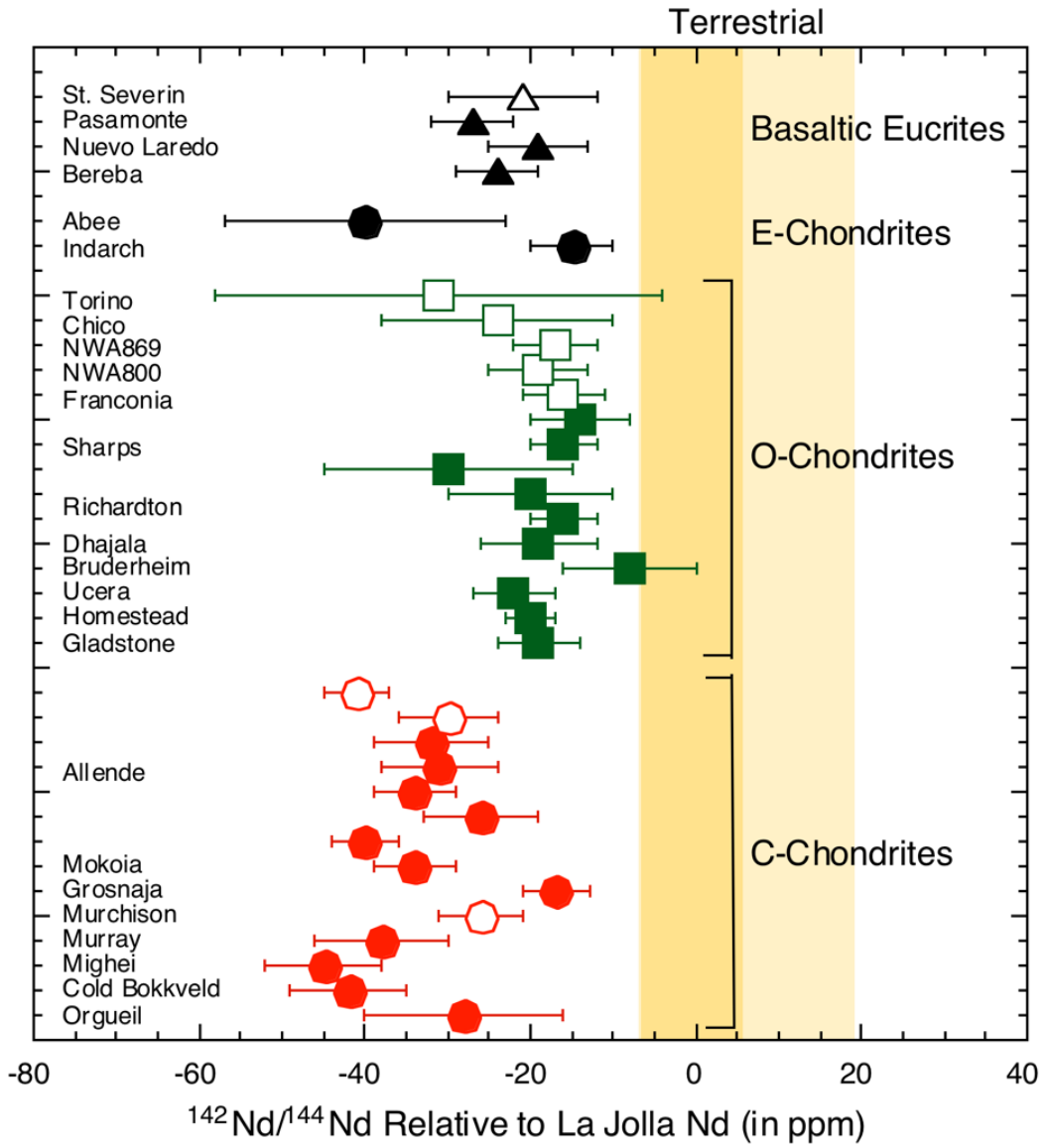

Figure 2: Deviations in $^{142}Nd/^{144}Nd$ for a variety of meteorites expressed in $\mu^{142}Nd$, or parts per million difference relative to the average value of the terrestrial La Jolla neodymium standard. The dark yellow bar shows the average and 2σ $\mu^{142}Nd$ values for standards and all terrestrial rocks younger than 3.6 Ga. The light yellow bar shows the range observed for Archaean samples (Boyet *et al.*, 2003; Caro *et al.*, 2003, 2006; Boyet and Carlson, 2006; Bennett *et al.*, 2007). Meteorite data are from Boyet and Carlson (2005) and Carlson *et al.* (2007) (filled symbols) and Nyquist *et al.* (1995); Andreasen and Sharma (2006); Rankenburg *et al.* (2006) (open symbols). After Carlson and Boyet (2008), used with permission.

closer to that of what is seen in terrestrial rocks today. Second, and alternatively, there could exist an unsampled reservoir deep within in the Earth that contains material with an even more negative ("subchondritic") ϵ^{142}Nd value that offsets the superchondritic ϵ^{142}Nd value of the mantle and crust, such that the bulk silicate Earth composition would have a chondritic ϵ^{142}Nd value. If the latter assumption is correct, how would this unsampled, ϵ^{142}Nd enriched reservoir have formed during the Earth's formation and solidification?

Carlson and Boyet (2008) propose that a hidden mantle reservoir, which does not participate in mantle convection and is enriched in neodymium and samarium, could resolve the terrestrial excess of neodymium isotopes compared to chondrite meteorites, assuming that the Earth formed with chondritic abundances for these refractory lithophile elements.

The D″ is a candidate for this proposed enriched mantle reservoir due to its high density contrast with the material above it in the mantle. Because of its high density and likely negative melt buoyancy (Knittle, 1998) this layer is predicted to not participate in mantle convection and thus would retain its initial concentrations of rare-Earth elements (REEs), specifically those of samarium and neodymium, over the age of the Earth without mixing with the rest of the mantle.

Elkins-Tanton (2008) explored the solidification of magma oceans on Earth and Mars, as well as the creation of and timescales for atmosphere generation. This model uses known mineral stabilities as a function of pressure to determine at what depth assemblages will solidify in the mantle, and while tracking both evolving liquid compositions of and trace element concentrations in the whole-mantle magma ocean. Here we extend the model from Elkins-Tanton (2008) to investigate the formation and composition of a deep, dense layer in the terrestrial mantle formed during magma ocean solidification, and whether the present concentrations of rare-Earth elements such as neodymium and samarium are consistent with the bulk silicate Earth composition originating from chondritic meteorites.

Also discussed is whether the properties of the deep dense layer produced in this model are consistent with enriched reservoir predictions, as well as the current

D″ layer. In Section 2, the model used by Elkins-Tanton (2008) and in this work is described. In Section 3 the formation of a deep dense layer by this model is discussed, especially regarding stability of this layer and its concentrations of rare-earth elements. In Section 4 we comment on the significance of the REE concentrations in this deep dense layer, and in Section 5 we discuss the implications of our results.

2 Methods

In this section we present a brief description of the methods used by Elkins-Tanton (2008) (hereafter the E-T2008 model) to model terrestrial magma ocean solidification, the assumptions used in this paper, as well as an overview of how the model treats the solidification and eventual overturn of the terrestrial magma ocean and fractionation of minerals therein.

We assume in this work that the entire mantle has been in a fully-molten, magma ocean stage. Several workers (including Smith *et al.*, 1970; Wood *et al.*, 1970; Warren, 1985; Tonks and Melosh, 1993) suggest that an impactor-created full-mantle magma ocean is not likely, and recent work by Canup (2008) predicts that impactors would melt up to 2000 km of the Earth's mantle, thus creating a deep, but not full-mantle, magma ocean. Although a single impactor would not have provided sufficient energy to melt the entire mantle at its present depth, it is assumed that the entirety of the mantle experienced a magma ocean state during Earth's accretion, and thus a whole-mantle terrestrial magma ocean assumption is made for this work.

Regarding composition of the magma ocean, the oxide species used in the E-T2008 model are silicon dioxide, aluminum oxide, iron oxide, magnesium oxide, and calcium oxide (Table 1); and the trace elements used in this thesis, which vary from those used in the E-T2008 model, are samarium, neodymium, thorium, and uranium (Table 2). Samarium and neodymium are used in this work, as opposed to lutetium and hafnium, as we can compare the concentrations of the former two elements to results from Boyet and Carlson (2005) and Carlson and Boyet (2008). The initial mass percents for the oxides are from Hart and Zindler (1986), reflecting the composition of the bulk silicate Earth (bulk silicate Earth), and the initial mass percents for the trace elements are from Anders and Grevesse (1989).

Table 1: Initial Magma Ocean Composition: Major Element Oxides

Species	SiO_2	Al_2O_3	FeO	MgO	CaO
Weight % Composition	45.96	4.06	7.54	37.78	2.31

Table 2: Initial Magma Ocean Composition: Trace Elements

Species	Sm	Nd	Th	U
Weight % Composition	1.472×10^{-5}	4.524×10^{-5}	2.94×10^{-6}	8.1×10^{-7}

The magma ocean is divided into 1,000 shells of equal volume, as this number of layers provides sufficient resolution to investigate mineral assemblages without being overly taxing on laptop processors. The magma ocean is also divided into eight larger ("meta") layers defined by a specific range of pressures and minerals that can exist at these pressures and depths (Figure 3). The shells are solidified from the magma ocean bottom to the near-surface.

During fractionation inside the meta-layers, the bulk composition of the equilibrium mineral is calculated, as is the whole mineral assemblage's Mg number (Equation 3). The Mg number, or magnesium number, of a mineral or rock is the ratio of the mineral's magnesium to magnesium plus iron atoms, on a molar basis.

$$\text{Mg \#} = \text{molar}\left(\frac{\text{Mg}}{\text{Mg + Fe}}\right) \tag{3}$$

Using experimentally determined exchange coefficients, the equilibrium composition of each mineral is calculated at each step in solidification. Equilibrium between liquid and solid is defined by the exchange coefficient K_D—the molar ratio between Fe and Mg in the solid mineral and Fe and Mg in the liquid (Equation 4).

$$K_D = \text{molar}\left[\frac{\left(\frac{\text{FeO}}{\text{MgO}}\right)_{solid}}{\left(\frac{\text{FeO}}{\text{MgO}}\right)_{liquid}}\right]. \tag{4}$$

Because the Fe-Mg exchange coefficient is less than one for the minerals used in this model, assemblages that crystallize have a higher Mg/Fe ratio than the melt out of which they solidify. After the melt begins to be depleted in magnesium, iron-rich members of a mineral series begin crystallizing. Thus, when solidification of the mantle is complete, the density profile of the mantle is such that lower density

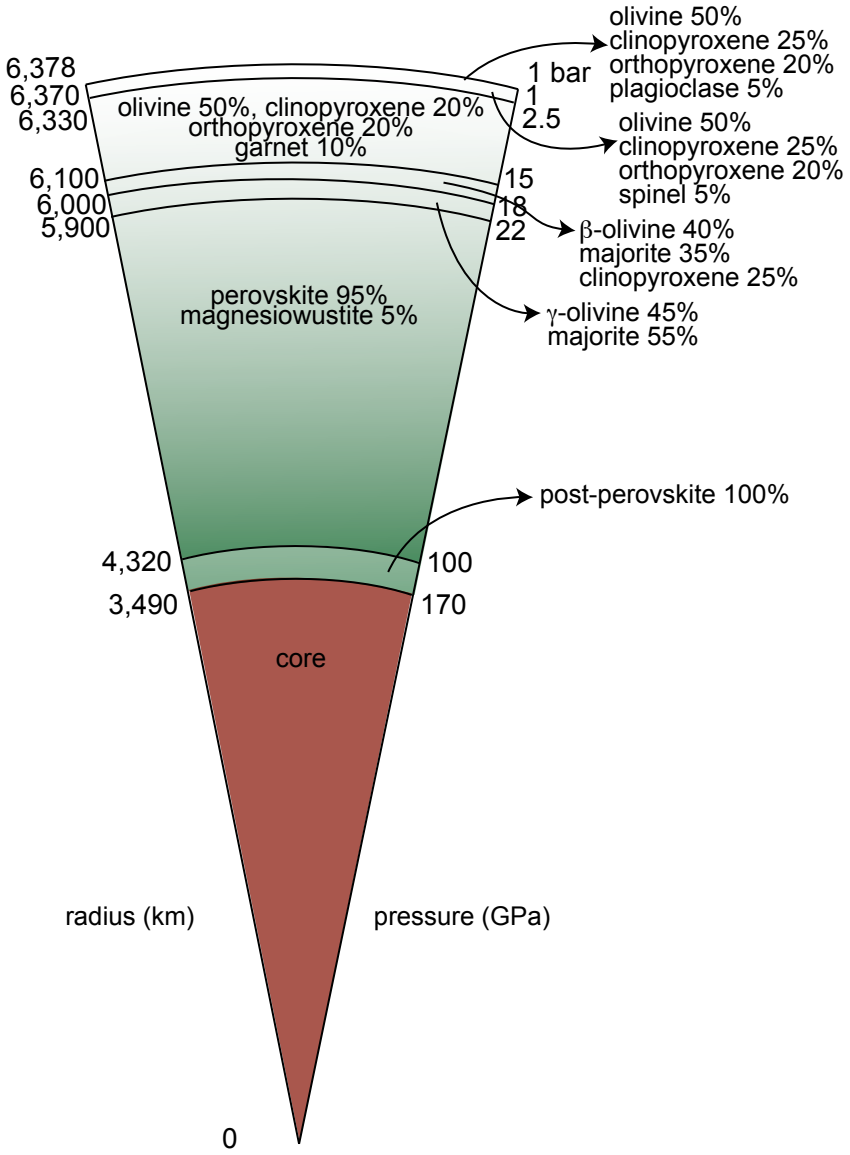

Figure 3: Mineral assemblages by depth which solidify from a full-Earth magma ocean in this model. The percentage of each pressure/depth range occupied by a particular assemblage is given on the right side of the figure. After Elkins-Tanton (2008).

cumulates are near the bottom of the solidified ocean, and higher density cumulates are clustered at the near-surface of the ocean.

As cumulates fractionate out of the melt, it is assumed that the bulk composition of these minerals is isolated from the melt, and that the composition of these solids remains constant and does not change as the solidification process proceeds.

The composition of the solidified layer is subtracted from the remaining magma ocean liquids at each step, resulting in an evolving magma ocean composition. As the solidification process occurs on a short timescale (as short as 10,000 years, Elkins-Tanton, 2008), it is thus assumed that there is no mixing between solidified layers. Any mixing among layers would be caused by density differences of assemblages due to differences in compositions at different depths.

As solidification progresses, incompatible elements become concentrated in the remaining liquids of the magma ocean. In this work, emphasis is placed on incompatible elements, defined as having a distribution coefficient, D, less than 1 (Albarède, 2003). Incompatible elements are species that occasionally fit into the cation sites of minerals, such as olivine, replacing iron or magnesium. Due to either a difference in charge or ionic radii, some incompatible elements do not enter the cation sites of minerals and thus become relatively enriched in the magma melt.

For this analysis, the incompatible elements used are rare earth elements, which are characterized by having charges higher than the ions they replace in the mineral lattice (Albarède, 2003). Thus, at the near surface of the magma ocean, the residual liquids become enriched in these incompatible rare Earth elements.

Due to convection, the temperature in the melted mantle varies adiabatically with depth. It is assumed that the entire mantle is molten from the core to the surface; in other words, the entire mantle is initially above the liquidus.

The melting temperature of the bulk silicate mantle depends on the pressure of material in the magma ocean, as well as the solidus temperature of melting initiation. This solidus used in this work is based on one calculated by Abe (1997) and the model used by Elkins-Tanton (2008), and hybridizes these two solidi to create a new model which is believed to be physically reasonable at both high and low temperatures and

pressures.

An adiabatic temperature profile is the curve that describes how temperature varies with pressure under adiabatic expansion conditions. Adiabatic processes are characterized by not giving or receiving heat, or by constant entropy; most mantle processes occur at approximately constant entropy (Asimow, 1999).

The adiabat is steeper than the solidus and the two curves intersect at the bottom of the mantle. At their intersection point, solidification begins, and therefore in the model used, solidification proceeds from the base of the magma ocean toward the surface. If the adiabat were more shallow, it would not intersect the solidus until closer to the surface of the planet.

Solidification begins at the bottom of the magma ocean with magnesium-bearing minerals crystallizing preferentially over iron-bearing minerals during magma ocean solidification. Mantle solidification proceeds up through the mantle, with the density of minerals calculated as a function of temperature and composition at specific pressures (Figure 3). These densities are calculated at a reference pressure of 1 atmosphere, and in the mantle at depth these pressures would be far greater. The reference pressure used in calculations is useful for comparing material at different pressures from across the mantle and for ordering material by density. As crystallization progresses from the bottom of the mantle to the surface, the density profile of the mantle reflects assemblages with lighter densities at the bottom of the mantle and denser assemblages closer to the surface (Figure 4). While the model does not solidify the last 0.3% by volume of the solidified mantle, it is assumed that at the end of solidification these remaining liquids solidify along with the rest of the mantle.

The density of each mineral is calculated by passing the Mg number, pressure, and temperature of the relevant mineral to an equation of state used for calculating the volume of solids. The widely-adopted equation of state used in the model is the Birch-Murnaghan equation (Equation 5). Its long use in geophysics has given it a "certain authority in the literature" (Anderson, 1995). In this equation, P is pressure, T is temperature, K_{0T} is the bulk modulus material at a pressure of $P = 0$ and a constant temperature, K'_0 is the bulk modulus pressure derivative at $P = 0$, and

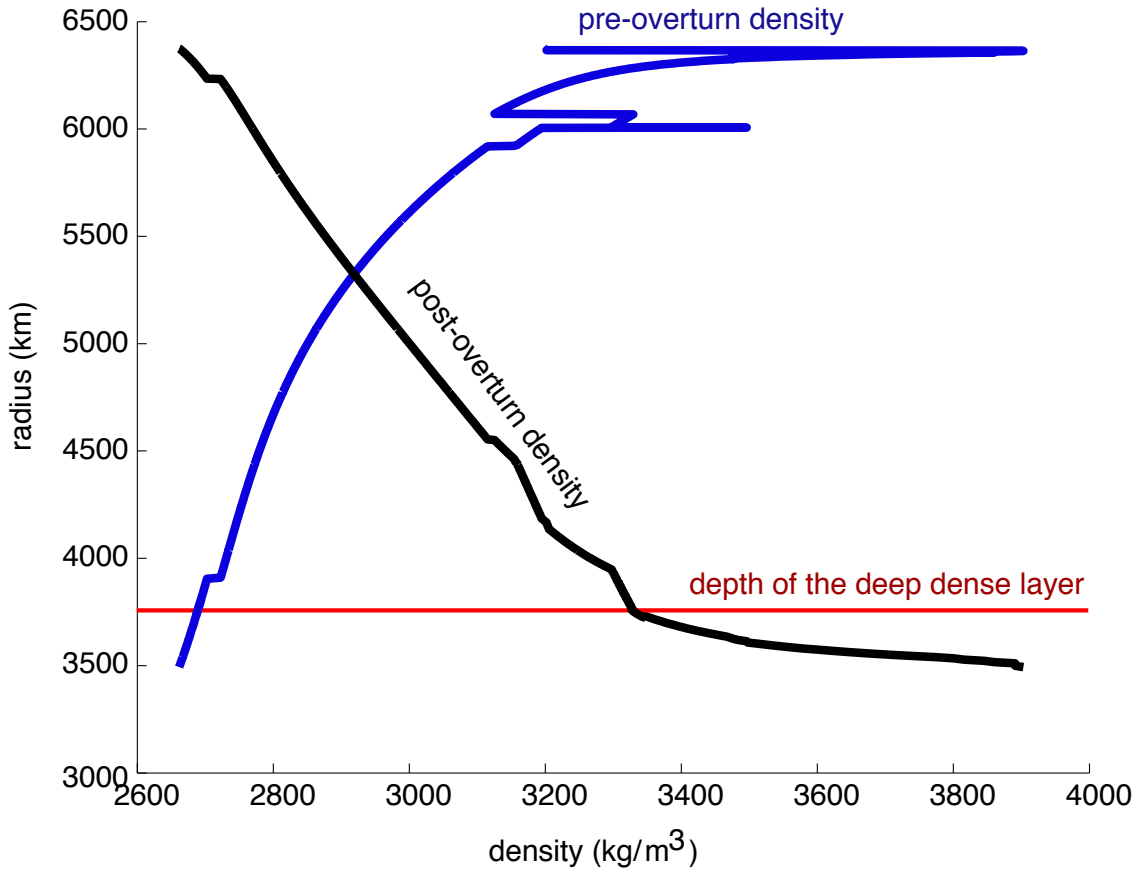

Figure 4: Density before (blue line) and after (black line) overturn. The pre-overturn density profile shows lighter assemblages toward the bottom of the solidified magma ocean, and heavier assemblages towards the near surface, as members of mineral series enriched in magnesium crystallize preferentially out of a melt. Density increases as iron-bearing minerals crystallize after magnesium-rich members. This density profile is unstable gravitationally, and results in an overturn event, where we assume that minerals are sorted by density. These densities are calculated at a reference pressure of 1 atmosphere, and in the mantle at depth these pressures would be far greater. The reference pressure used in calculations is useful for comparing material at different pressures from across the mantle and for ordering material by density. The maximum radial extent of the deep dense layer at 3760 km is indicated (red line).

V/V_0 is the ratio of the volume of a solid at a specific temperature to its equilibrium volume.

The bulk modulus is defined as $K = -V\left(\frac{\partial P}{\partial V}\right)_T$ and is thus proportional to changes in pressure with respect to volume at constant temperature; it is the amount of pressure increase required to cause a parcel of matter to decrease in relative volume.

$$P = \frac{3K_{0T}}{2}\left[\left(\frac{V}{V_0}\right)^{7/3} - \left(\frac{V}{V_0}\right)^{5/3}\right]\left\{1 + \frac{3}{4}(K_0' - 4)\left[\left(\frac{V}{V_0}\right)^{2/3} - 1\right]\right\} \tag{5}$$

The Birch-Murnaghan equation is arranged such that when the correct volume ratio is provided for a mineral (given the mineral's specific pressure, temperature, bulk modulus, and bulk modulus pressure derivative), the equation returns the relevant volume ratio for the specified pressure and temperature. The mass of each mineral is then divided by the volume it occupies, yielding a density for each mineral.

Including these residual layers of unsolidified material, the resulting density profile of the solidified magma ocean is gravitationally unstable, which leads to the cumulates undergoing an overturn event to a more gravitationally stable configuration. Overturn is assumed to occur rapidly (Elkins-Tanton, 2008) via Rayleigh-Taylor instabilities (Elkins-Tanton *et al.*, 2011), and that, after overturn, cumulates are sorted by density, with the higher density cumulates sinking toward the bottom of the magma ocean and the lighter cumulates rising toward the near surface of the solidified magma ocean.

3 Results

Stability of the Deep Dense Layer As a result of sorting by density during overturn, a dense layer of material sinks to the bottom of the solidified magma ocean. In the model used, the densest materials that sink to the bottom of the solidified magma ocean during overturn form a layer approximately 250 km thick. This thickness of this deep dense layer is determined by inspecting the density profile of the magma ocean after overturn. A discontinuity in the density profile slope leads us to define material denser than 3,320 kg/m^3 to be part of the deep dense layer (Figure 4). The mass of this layer, calculated by integrating the densities of assemblages in this layer over the range of radii the layer occupies, is 1.9×10^{23} kg, which is 3.24% of the mantle by mass.

In order for the deep dense layer material to participate in mantle convection and thus be reentrained by the mantle, the material would have to undergo a negative change in density. In order to have a lower density, the material would have to expand. We consider a solid material that expands linearly (Equation 3) where the change in density for a material with thermal expansion coefficient of $\alpha = 10^{-5}$ K^{-1}, change in temperature ΔT, and initial density ρ_i.

$$\Delta\rho = \Delta T \alpha \rho_i \tag{6}$$

The deep dense layer's density is between 3,300 and 3,900 kg/m^3, as calculated at a reference pressure of 1 atmosphere (at pressure the densities of assemblages in this layer are higher). For the material at a density of 3,300 kg/m^3 a temperature change of upwards of 5,000 K would be require to expand this material to a density of 3,100 kg/m^3 (Figure 5). Williams and Jeanloz (1990); Lay *et al.* (1998) predict a temperature change on the order of 1,000 K across the D″ layer, so this figure is not unreasonable. A larger temperature change would be required to expand material at greater densities such that it would be able to mix with the mantle.

Assuming that material with a density lower than 3,330 kg/m^3 is reentrained by the mantle, this would change the mass of the deep dense layer to be 1.7×10^{23} kg,

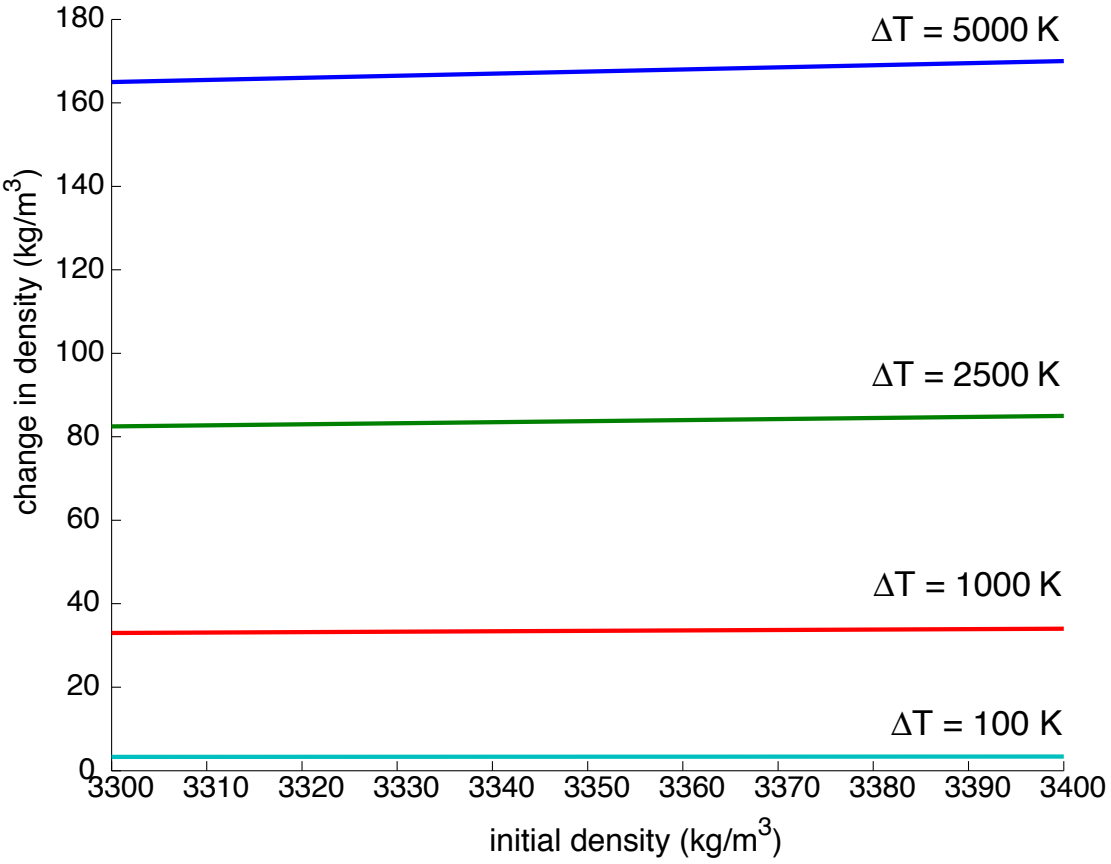

Figure 5: Temperature-based stability of material in the deep dense layer. In order to achieve a change of 200 kg/m^3 in density of the deep dense layer such that the material would participate in mantle convection, a change in temperature of upwards of 5,000 K is required. The dotted lines represent constant density.

which is 2.8% of the mantle by mass. As a change in temperature on the order of 1000 K is required for the expansion that would yield this sort of density change, it is not likely that heating of the lighter material in this region would cause appreciable changes in the bulk physical properties of the deep dense layer that forms.

Even if material in this layer were to melt, for example from radiogenic heating, it would very likely be negatively buoyant in comparison to the cumulates residing above it (Knittle, 1998), and it is thus unlikely that this melt would participate in mantle convection. As a result, this deep dense layer is stable against participation in mantle convection, and could remain at the base of the solidified magma ocean for the age of the Earth.

μ^{142}Nd values for the Deep Dense Layer We can calculate the overall deep dense layer's concentrations of rare-Earth elements—samarium, neodymium, uranium, and thorium—by averaging the weight percentages of these species across the volume of the deep dense layer. Because Sm and Nd are incompatible, they become enriched in the final liquids.

The overturn process sorts mantle cumulates by density, resulting in a mantle density profile that increases with depth. Distributed throughout the mantle are the rare-Earth elements samarium, neodymium, thorium, and uranium. Using the abundances of rare-Earth elements throughout the post-overturn mantle, the weight percent of a particular element in the mantle or deep dense layer can be obtained. The model used tracks the weight percentages of elements, not specific isotopes, so the abundances of ^{142}Nd and ^{144}Nd must be calculated in order to determine μ^{142}Nd (Equation 2) for the mantle reservoirs. To calculate μ^{142}Nd values for the mantle and deep dense layer, first the ^{142}Nd/^{144}Nd values for both reservoirs must be determined. For example, to obtain the concentration of ^{142}Nd in a reservoir (Equation 7), we multiply the weight percent of the element by its isotopic abundance (values from Zhao *et al.*, 2005) and divide by its molar mass.

$$[^{142}\text{Nd}] = \text{weight \% Nd} \times 0.272 \ / \ 144.242 \tag{7}$$

The $^{142}Nd/^{144}Nd$ values for chondritic and terrestrial standards are well known, and so these are evolved from their initial concentrations at 4.567 Ga (the formation time of the soldest solar system solids (Connelly *et al.*, 2008)) to present day values. In this model the neodymium and samarium isotope concentrations are evolved as in one reservoir until 4.5 Ga when the Moon-forming giant impact (Hartmann and Davis, 1975) is posited to have occurred (Lee *et al.*, 1997). At this point, the mantle is split into the deep dense layer and the present-day mantle and the concentrations of neodymium and samarium in these reservoirs evolve independently.

The evolving $^{142}Nd/^{144}Nd$ values for the mantle and deep dense layer are calculated by adding the amount of ^{146}Sm that decays to ^{142}Nd over the age of the Earth to the initial amount of ^{142}Nd in the reservoir, then dividing the amount of ^{142}Nd by ^{144}Nd to obtain the $^{142}Nd/^{144}Nd$ ratio.

Once the $^{142}Nd/^{144}Nd$ ratio of the reservoir in question is calculated, it is then compared to the terrestrial La Jolla standard, with an $^{142}Nd/^{144}Nd$ ratio of 1.141840 (Boyet and Carlson, 2005). Subtracting 1 and multiplying by 1,000,000 yields the $\mu^{142}Nd$ value for the reservoir, which can be compared to the predicted $\mu^{142}Nd$ values from Carlson and Boyet (2008).

The resulting $\mu^{142}Nd$ values for both the deep dense layer (to be compared to the early enriched reservoir predicted by Carlson and Boyet (2008)) and the mantle (to be compared to the early depleted reservoir from Carlson and Boyet (2008)) returned by our model depend heavily on the concentrations of Nd and Sm in both the deep dense layer and the mantle, and thus, on the distribution coefficients of these rare-Earth elements for mantle minerals. Much of the mantle post-solidification is occupied by mantle perovskite, for which the distribution coefficients of Sm, Nd, Th, and U are not well constrained (Elkins-Tanton, 2008, and supplemental material referenced therein).

To explore the effects of small changes in the distribution coefficients for rare-Earth elements, a Monte Carlo simulation was run, varying the distribution coefficients for both Ca- and MgFe-perovskite from their minimum to maximum values in the literature (Tables 3 and 4; assuming that Al-perovskite has the same distribution coefficients as MgFe-perovskite). One thousand different combinations of distribution

coefficients for Ca- and MgFe-perovskite were passed to the model in order to return a range of possible μ^{142}Nd values. Distribution coefficients used in these simulations for samarium in MgFe-perovskite are represented on the color scale: dark brown represents a D of close to 0.01, while light brown represents a D near 0.5.

Table 3: REE Partition Coefficients for Calcium Perovskite

Species	Minimum	Maximum	Reference
Sm	1.0	5	Kato *et al.* (1988); Corgne and Wood (2005); Corgne *et al.* (2005)
Nd	1	10	Kato *et al.* (1988); Corgne *et al.* (2005)
U	0.01	1	Kato *et al.* (1988); Corgne and Wood (2005); Corgne *et al.* (2005)
Th	1.0	10	Corgne and Wood (2005); Corgne *et al.* (2005)

Table 4: REE Partition Coefficients for MgFe Perovskite

Species	Minimum	Maximum	Reference
Sm	0.01	0.5	Corgne *et al.* (2005); Liebske *et al.* (2005)
Nd	0.01	0.02	Corgne *et al.* (2005)
U	0.01	1.0	Corgne *et al.* (2005); Liebske *et al.* (2005)
Th	0.01	0.2	Corgne *et al.* (2005); Liebske *et al.* (2005)

Carlson and Boyet (2008) predicts that for an early enriched reservoir occupying 4% of the mantle mass, the resulting μ^{142}Nd value should be -54, with that of the early depleted reservoir (mantle minus early enriched reservoir composition) being 0. The results of this Monte Carlo simulation (Figure 6) show that this predicted combination of μ^{142}Nd values is not possible. These results are inconsistent with a chondritic initial bulk silicate Earth composition, the implications of which will be discussed further in Section 4.

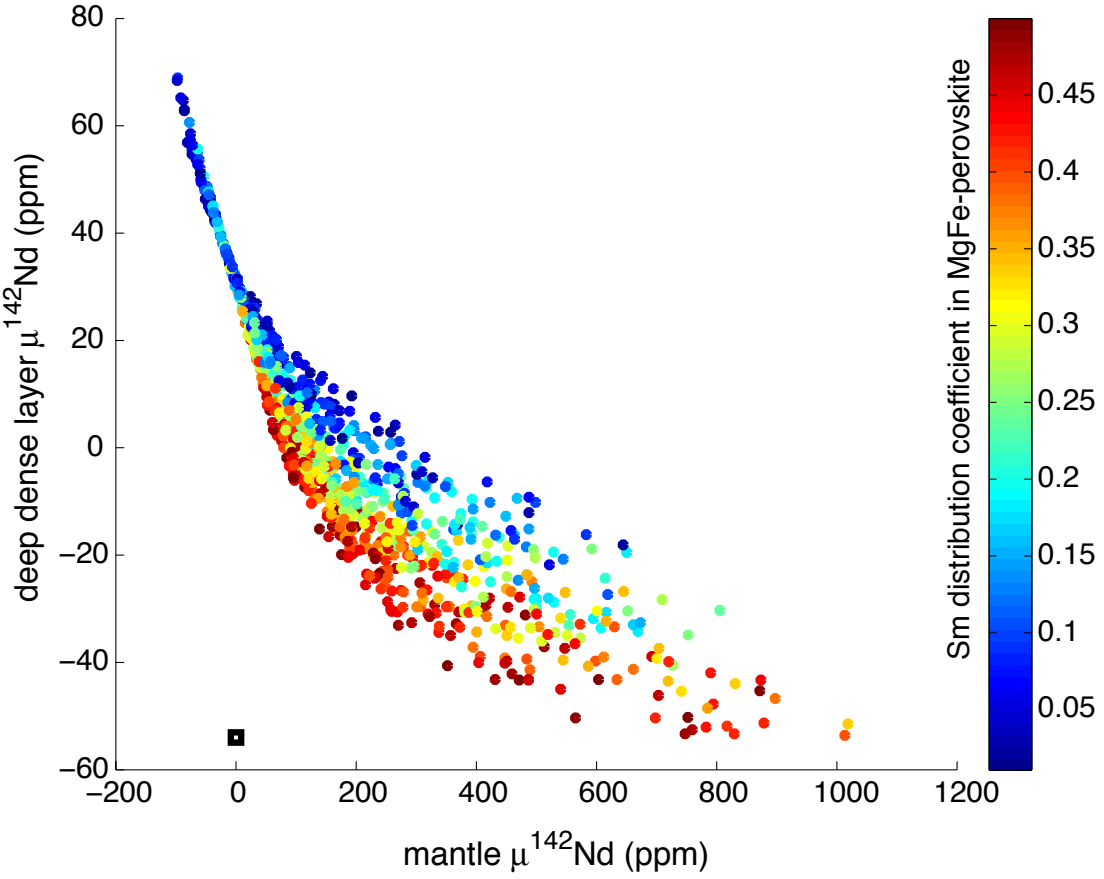

Figure 6: The μ^{142}Nd values for the model's mantle and deep dense layer from a 1000-run Monte Carlo simulation in which the distribution coefficients for Sm, Nd, U, Th, OH, and CO in mantle Ca- and MgFe-perovskite were varied, resulting in different mantle and deep dense layer concentrations of Sm and Nd. The box at (0, -54) represents the predicted μ^{142}Nd values for the EDR and EER from Carlson and Boyet (2008). The variation in color represents the different initial distribution coefficient values of Sm in MgFe perovskite (Table 4), with blue being small and red being large initial distribution coefficients.

4 Discussion

Carlson and Boyet (2008) predicts that the μ^{142}Nd value for the early enriched reservoir that is 4% by mass of the mantle is -54, indicating a layer highly enriched in ^{142}Nd compared to terrestrial rocks. If our model agrees with that of Carlson and Boyet (2008), we would expect our deep dense layer layer to have a similar μ^{142}Nd ratio. However, the model used in this work produces μ^{142}Nd values for the deep dense layer that show over enrichment in ^{146}Sm and thus excessively large μ^{142}Nd values for the deep dense layer when μ^{142}Nd of the mantle is 0 (Figure 6). If the early depleted reservoir and the mantle are the same reservoir, and thus the source region for the terrestrial ^{142}Nd/^{144}Nd standard, by definition they should have a μ^{142}Nd value of 0.

Assuming both formed from the same chondritic source, it is also not possible to have an early enriched reservoir with a positive μ^{142}Nd value and an early depleted reservoir with 0. This would be only possible if the early enriched reservoir is negligible in mass compared to the early depleted reservoir (which it is not in the model used, at 4% of the mantle mass), and also does not contain enough REEs to change the Sm/Nd ratio of the early depleted reservoir by enough to create an appreciable change in ^{142}Nd for the early depleted reservoir.

Inspecting Figure 6 further, some of the solutions have positive μ^{142}Nd values in both the deep dense layer and mantle. Mass balance dictates that splitting a source with an initial chondritic samarium to neodymium ratio into two reservoirs with higher than chondritic (and therefore positive) samarium to neodymium ratios is not physically possible.

Even though the Sm and Nd concentrations and μ^{142}Nd values for the deep dense layer produced by our model are not consistent with those predicted by Carlson and Boyet (2008), the physical properties of this layer match those from other workers. Specifically, the height of this layer (250 km) matches literature thickness predictions (Kendall and Shearer, 1994; Garnero, 2000; Oganov and Ono, 2004; Wentzcovitch *et al.*, 2006; Youngs and Houseman, 2007), and the high density contrast of this layer with the material above it is consistent with predictions from Knittle (1998).

The density of this layer also means that it is stable against expansion due to increases in temperature. As a temperature change of 5,000 K would be required to expand this deep dense layer, the assumption that the majority of this layer does not participate in mantle convection and therefore that its budget of Nd and Sm would be preserved over the age of the Earth is plausible.

5 Conclusions

We showed that a crystallizing magma ocean can produce a deep mantle reservoir that is stable against being mixed with the mantle over timescales similar to the age of the Earth. Even if this layer were to increase in temperature, it is likely that the change in volume and thus density would be insufficiently large for the material in this reservoir to mix with the overlying mantle.

While we can explain the formation of a stable dense basal layer with the model used in this work, we cannot produce isotope concentrations in this lower-mantle reservoir that match predictions consistent with the Earth's mantle having formed with a chondritic composition. The concentrations of Sm and Nd in this deep dense layer suggest that an overabundance of samarium produced during solidification by the model could be responsible for increasing the μ^{142}Nd of the deep dense layer to the point where it is super-chondritic and inconsistent with having evolved from a chondritic source. Thus, we are not able to verify via the ^{146}Sm $/^{142}$Nd system whether the BSE composition is consistent with a chondritic terrestrial mantle origin.

Part of the discrepancy between the results of this study and the prediction of Carlson and Boyet (2008) regarding the μ^{142}Nd values of the mantle and deep dense layer is that the latter workers use a slightly different set of abundances for their BSE composition (McDonough and s. Sun (1995) versus Anders and Grevesse (1989) and Hart and Zindler (1986) in this work). While the deviations between the chondritic BSE values used are small, they could have a small effect on the final μ^{142}Nd values calculated by this work.

References

Abe, Y. 1997. Thermal and chemical evolution of the terrestrial magma ocean. *Physics of the Earth and Planetary Interiors 100*(1-4), 27–39.

Albarède, F. 2003. *Geochemistry: an introduction*. Cambridge University Press.

Amelin, Y., and E. Rotenberg 2004. Sm-Nd systematics of chondrites. *Earth and Planetary Science Letters 223*(3-4), 267–282.

Anders, E., and N. Grevesse 1989. Abundances of the elements - Meteoritic and solar. *Geochimica et Cosmochimica Acta 53*(1), 197–214.

Anderson, O. 1995. *Equations of state of solids for geophysics and ceramic science*. Oxford Monographs on Geology and Geophysics. Oxford University Press.

Andreasen, R., and M. Sharma 2006. Solar nebula heterogeneity in p-process samarium and neodymium isotopes. *Science 314*(5800), 806–809.

Asimow, P. D. 1999. Melting the mantle. In H. Sigurdsson (Ed.), *Encyclopedia of Volcanoes*, pp. 55–68. Academic Press.

Beatty, J., C. Petersen, and A. Chaikin 1999. *The New Solar System*. Cambridge University Press.

Bennett, V. C., A. D. Brandon, and A. P. Nutman 2007. Coupled ^{142}Nd-^{143}Nd isotopic evidence for hadean mantle dynamics. *Science 318*(5858), 1907–1910.

Boyet, M., J. Blichert-Toft, M. Rosing, M. Storey, P. Télouk, and F. Albarède 2003. ^{142}Nd evidence for early Earth differentiation. *Earth and Planetary Science Letters 214*(3-4), 427–442.

Boyet, M., and R. W. Carlson 2005. ^{142}Nd Evidence for Early (>4.53 Ga) Global Differentiation of the Silicate Earth. *Science 309*(5734), 576–581.

Boyet, M., and R. W. Carlson 2006. A new geochemical model for the Earth's mantle inferred from ^{146}Sm-^{142}Nd systematics. *Earth and Planetary Science Letters 250*(1-2), 254–268.

Canup, R. M. 2008. Accretion of the Earth. *Philosophical Transactions of the Royal Society A: Mathematical, Physical and Engineering Sciences 366*(1883), 4061–4075.

Carlson, R. W., and M. Boyet 2008. Composition of the Earth's interior: the importance of early events. *Philosophical Transactions of the Royal Society A: Mathematical, Physical and Engineering Sciences 366*(1883), 4077–4103.

Carlson, R. W., M. Boyet, and M. Horan 2007. Chondrite barium, neodymium, and samarium isotopic heterogeneity and early Earth differentiation. *Science 316*(5828), 1175–1178.

Caro, G., B. Bourdon, J.-L. Birck, and S. Moorbath 2003. ^{146}Sm-^{142}Nd evidence from Isua metamorphosed sediments for early differentiation of the Earth's mantle. *Nature 423*(6938), 428–432.

Caro, G., B. Bourdon, J.-L. Birck, and S. Moorbath 2006. High-precision 142nd/144nd measurements in terrestrial rocks: Constraints on the early differentiation of the Earth's mantle. *Geochimica et Cosmochimica Acta 70*(1), 164–191.

Chambers, J. E. 2004. Planetary accretion in the inner solar system. *Earth and Planetary Science Letters 223*(3-4), 241–252.

Connelly, J. N., Y. Amelin, A. N. Krot, and M. Bizzarro 2008. Chronology of the Solar System's Oldest Solids. *Astrophysical Journal, Letters 675*(2), L121–L124.

Corgne, A., C. Liebske, B. J. Wood, D. C. Rubie, and D. J. Frost 2005. Silicate perovskite-melt partitioning of trace elements and geochemical signature of a deep perovskitic reservoir. *Geochimica et Cosmochimica Acta 69*(2), 485–496.

Corgne, A., and B. Wood 2005. Trace element partitioning and substitution mechanisms in calcium perovskites. *Contributions to Mineralogy and Petrology 149*(1), 85–97.

DePaolo, D. J., and G. J. Wasserburg 1976. Nd isotopic variations and petrogenetic models. *Geophysical Research Letters 3*(5), 249–252.

Elkins-Tanton, L. T. 2008. Linked magma ocean solidification and atmospheric growth for Earth and Mars. *Earth and Planetary Science Letters 271*(1-4), 181–191.

Elkins-Tanton, L. T., S. Burgess, and Q.-Z. Yin 2011. The lunar magma ocean: reconciling the solidification process with lunar petrology and geochronology (abstract #1505). In *Proc. 42nd Lunar and Planetary Science Conf.*, Volume XLII. Lunar and Planetary Institute, Houston.

Garnero, E. 2000. Heterogeneity of the lowermost mantle. *Annual Review of Earth and Planetary Sciences 28*(1), 509–537.

Hart, S. R., and A. Zindler 1986. In search of a bulk-Earth composition. *Chemical Geology 57*(3-4), 247–267.

Hartmann, W. K., and D. R. Davis 1975. Satellite-sized planetesimals and lunar origin. *Icarus 24*(4), 504–514.

Kato, T., A. Ringwood, and T. Irifune 1988. Experimental determination of element partitioning between silicate perovskites, garnets and liquids: constraints on early differentiation of the mantle. *Earth and Planetary Science Letters 89*(1), 123–145.

Kendall, J.-M., and P. M. Shearer 1994. Lateral variations in D double prime thickness from long period shear wave data. *Journal of Geophysical Research 99*(B6), 11,575–11,590.

Knittle, E. 1998. The solid/liquid partitioning of major and radiogenic elements at lower mantle pressures: implications for the core-mantle boundary region. In M. Gurnis, M. E. Wysession, E. Knittle, and B. A. Buffett (Eds.), *The Core-Mantle Boundary Region*, Geodynamics Series 28, pp. 119–130. American Geophysical Union Press.

Lay, T., Q. Williams, and E. Garnero 1998. The core-mantle boundary layer and deep Earth dynamics. *Nature 392*(6675), 461–468.

Lee, D.-C., A. N. Halliday, G. A. Snyder, and L. A. Taylor 1997. Age and origin of the moon. *Science 278*(5340), 1098–1103.

Liebske, C., B. Schmickler, H. Terasaki, B. T. Poe, A. Suzuki, K. Funakoshi, R. Ando, and D. C. Rubie 2005. Viscosity of peridotite liquid up to 13 GPa: Implications for magma ocean viscosities [rapid communication]. *Earth and Planetary Science Letters 240*(3-4), 589–604.

Lugmair, G. W., T. Shimamura, R. S. Lewis, and E. Anders 1983. Samarium-146 in the Early Solar System: Evidence from Neodymium in the Allende Meteorite. *Science 222*(4627), 1015–1018.

Maji, S., S. Lahiri, B. Wierczinski, and G. Korschinek 2006. Separation of samarium and neodymium: a prerequisite for getting signals from nuclear synthesis. *Analyst* **131**, 1332–1334.

McDonough, W. F., and S. s. Sun 1995. The composition of the Earth. *Chemical Geology 120*(3-4), 223–253. Chemical Evolution of the Mantle.

Nyquist, L. E., H. Wiesmann, B. Bansal, C. Y. Shih, J. E. Keith, and C. L. Harper 1995. ^{146}Sm-^{142}Nd formation interval for the lunar mantle. *Geochimica et Cosmochimica Acta 59*(13), 2817–2837.

Oganov, A. R., and S. Ono 2004. Theoretical and experimental evidence for a post-perovskite phase of $MgSiO_3$ in Earth's D″ layer. *Nature 430*(6998), 445–448.

Rankenburg, K., A. D. Brandon, and C. R. Neal 2006. Neodymium isotope evidence for a chondritic composition of the moon. *Science 312*(5778), 1369–1372.

Raymond, S. N., D. P. O'Brien, A. Morbidelli, and N. A. Kaib 2009. Building the terrestrial planets: Constrained accretion in the inner solar system. *Icarus 203*(2), 644 – 662.

Ringwood, A. E. 1966. Chemical evolution of the terrestrial planets. *Geochimica et Cosmochimica Acta 30*(1), 41–104.

Rollinson, H. R. 2007. *Early Earth Systems: A Geochemical Approach*. Wiley-Blackwell.

Safronov, V. S. 1978. The heating of the Earth during its formation. *Icarus 33*(1), 3–12.

Smith, J. V., A. T. Anderson, R. Newton, E. Olsen, P. Wyllie, A. Crewe, M. Isaacson, and D. Johnson 1970. Petrologic history of the Moon inferred from petrography, mineralogy, and petrogenesis of Apollo 11 rocks. In *Proceedings of the Apollo 11 Lunar Science Confrence*, pp. 897–925.

Tonks, W. B., and H. J. Melosh 1993. Magma ocean formation due to giant impacts. *Journal of Geophysical Research 98*(E3), 5319–5333.

Warren, P. 1985. The magma ocean concept and lunar evolution. *Annual Review of Earth and Planetary Sciences 13*(1), 201–240.

Weidenschilling, S. J., D. Spaute, D. R. Davis, F. Marzari, and K. Ohtsuki 1997. Accretional Evolution of a Planetesimal Swarm. *Icarus 128*(2), 429–455.

Wentzcovitch, R., T. Tsuchiya, and J. Tsuchiya 2006. $MgSiO_3$ post-perovskite at D″ conditions. *Proceedings of the National Academy of Sciences 103*(3), 543–546.

Williams, Q., and R. Jeanloz 1990. Melting Relations in the Iron-Sulfur System at Ultra-High Pressures: Implications for the Thermal State of the Earth. *J. Geophys. Res. 95*(B12), 19299–19310.

Wood, J., J. Dickey Jr, U. Marvin, and B. Powell 1970. Lunar anorthosites and a geophysical model of the Moon. In *Proceedings of the Apollo 11 Lunar Science Confrence*, pp. 965–988.

Youngs, B. A., and G. A. Houseman 2007. Topography on the D″ region from analysis of a thin dense layer beneath a convecting cell. *Physics of The Earth and Planetary Interiors 160*(1), 60–74.

Zhao, M., T. Zhou, J. Wang, H. Lu, and F. Xiang 2005. Absolute measurements of neodymium isotopic abundances and atomic weight by MC-ICPMS. *International Journal of Mass Spectrometry 245*(1-3), 36–40.